

Highly efficient blue top-emitting device with phase-shift adjustment layer

Yanlong Meng, Wenfa Xie, Guohua Xie, Letian Zhang, Yi Zhao, *Jingying Hou, and Shiyong Liu¹

State Key Laboratory on Integrated Optoelectronics, College of Electronic Science and Engineering, Jilin University, Changchun 130012, China

¹syliu@jlu.edu.cn

*Corresponding author: mengyanlong@yeah.net

Abstract: The phase shift on the reflection from a semitransparent electrode of a top-emitting organic light-emitting device is utilized in this paper to realize a deep blue emission with high efficiency. The phase shift could be adjusted by changing the thickness of Alq₃ when it was deposited onto the semitransparent electrode of the device. Through simulation it is found that the blue shift of the resonant wavelength occurs in a certain range, which is concerned with Alq₃ thickness and the cavity length between two reflective electrodes. According to the simulation, a blue top-emitting organic light-emitting device with a designed structure was demonstrated experimentally by using such a phase-shift adjustment layer. Finally, the device showed excellent performance both in efficiency (3.4 cd/A at 8 V) and Commission Internationale de l'Eclairage coordinates (0.13, 0.15). The brightness of the device reached 20 000 cd/m².

© 2009 Optical Society of America

OCIS codes: (230.0230) Optical device; (230.5750) Resonators; (230.3670) Light-emitting diodes; (310.0310) Thin films; (310.6188) Spectral properties; (310.6805) Theory and design.

References and links

1. C.-W. Chen, C.-L. Lin, and C.-C. Wu, "An effective cathode structure for inverted top-emitting organic light-emitting devices," *Appl. Phys. Lett.* **85**, 2469–2471 (2004).
2. C. J. Lee, R. B. Pode, and J. I. Han, "Red electrophosphorescent top emission organic light-emitting device with Ca/Ag semitransparent cathode," *Appl. Phys. Lett.* **89**, 253508 (2006), <http://link.aip.org/link/?APPLAB/89/253508/1>.
3. D. G. Moon, R. B. Pode, C. J. Lee, and J. I. Han, "Efficient red electrophosphorescent top-emitting organic light-emitting devices," *Mater. Sci. Eng. B* **121**, 232–237(2005).
4. S. Han, C. Huang, and Z.-H. Lu, "Color tunable metal-cavity organic light-emitting diodes with fullerene layer," *J. Appl. Phys.* **97**, 093102 (2005), <http://link.aip.org/link/?JAPIAU/97/093102/1>.
5. H. J. Peng, J. X. Sun, X. L. Zhu, X. M. Yu, M. Wong, and H. S. Kwok, "High-efficiency microcavity top-emitting organic light-emitting diodes using silver anode," *Appl. Phys. Lett.* **88**, 073517 (2006).
6. S.-F. Hsu, C.-C. Lee, S.-W. Hwang, H.-H. Chen, C. H. Chen, and A. T. Hu, "Color-saturated and highly efficient top-emitting organic light-emitting," *Thin Solid Films* **478**, 271–274 (2005).
7. S.-F. Hsu, C.-C. Lee, A. T. Hu, and C. H. Chen, "Fabrication of blue top-emitting organic light-emitting devices," *Curr. Appl. Phys.* **4**, 663–666 (2004).
8. A. L. Burin and M. A. Ratner, "Exciton migration and cathode quenching in organic light emitting diodes," *J. Phys. Chem. A* **104**, 4704–4710 (2000).
9. C. L. Mitsas and D. I. Siapkas, "Generalized matrix method for analysis of coherent and incoherent reflectance and transmittance of multilayer structures with rough surfaces, interfaces, and finite substrates," *Appl. Opt.* **34**, 1678–1683 (1995).
10. A. B. Djurišić and A. D. Rakić, "Organic microcavity light-emitting diodes with metal mirrors: dependence of the emission wavelength on the viewing angle," *Appl. Opt.* **41**, 7650–7656 (2002).
11. D. G. Deppe, C. Lei, C. C. Lin, and D. L. Huffaker, "Spontaneous emission from planar microstructures," *J. Mod. Opt.* **41**, 325–344 (1994), <http://dx.doi.org/10.1080/09500349414550361>.
12. S. F. Chen, W. F. Xie, Y. L. Meng, P. Chen, Y. Zhao, and S. Y. Liu, "Effect of 2,9-dimethyl-4,7-diphenyl-1,10-phenanthroline outcoupling layer on electroluminescent performances in top-emitting organic light-emitting devices," *J. Appl. Phys.* **103**, 054506 (2008).

13. C.-C. Wu, C.-W. Chen, C.-L. Lin, and C.-J. Yang, "Advanced organic light-emitting devices for enhancing display performances," *J. Disp. Technol.* **1**, 248–265 (2005).
14. H. Becker, S. E. Burns, N. Tessler, and R. H. Friend, "Role of optical properties of metallic mirrors in microcavity structures," *J. Appl. Phys.* **81**, 2825–2829 (1997).

1. Introduction

Recently, top-emitting organic light-emitting devices (TEOLEDs) have attracted more and more attention because of their potential for commercial application in using more complicated active-matrix architectures for high-performance and fabrication of more pure light via the microcavity effect to accomplish full-color, active-matrix organic light-emitting devices (OLEDs) [1]. As is known, the spectra emitted by a TEOLED with double metallic electrodes could be narrowed easily because of the microcavity effect. As a result, the color of emissive light shows better saturation than that of conventional bottom-emitting devices. Up to now, most of the monochromatic TEOLEDs have exhibited better performance than that of corresponding bottom-emitting devices [2–5]. However, it is still difficult to obtain a pure blue TEOLED with high efficiency. Though most of blue TEOLEDs reported thus far have acceptable Commission Internationale de l'Éclairage coordinates ($CIE_{x,y}$), their efficiency is still not as good as that of corresponding bottom-emitting devices [6,7].

It is well known that the resonance wavelength of a cavity is a dominant factor in the determination of the emission wavelength of a device using such a microcavity structure. According to the resonant conditions of the microcavity, the resonance wavelength could be determined by the following formula:

$$\sum_i \frac{4\pi d_i n_i(\lambda)}{\lambda} - \varphi_{\text{top}}(0, \lambda) - \varphi_{\text{bot}}(0, \lambda) = 2m\pi, \quad (1)$$

where λ is the emission wavelength; $\varphi_{\text{top}}(0, \lambda)$ and $\varphi_{\text{bot}}(0, \lambda)$ are the angle- and wavelength-dependent phase changes on reflection from the top and bottom mirrors, respectively; and m is an integer that defines the mode number. $n_i(\lambda)$ and d_i are the refractive index and the thickness of each organic layer. From this formula, it is well understood that the achievement of a shorter resonance wavelength under a fixed mode requires a smaller cavity length or a bigger phase shift on the reflection. Though reducing the thickness of the organic medium between two reflective mirrors is a convenient method to realize the shorter resonant wavelength, it is unserviceable for application because of its many other problems [8]. To avoid those problems, another way to accomplish a blue top-emitting device with high efficiency is considered. Accordingly, a change in the phase shift on the reflection from a semitransparent electrode where light is emitted is discussed in this paper. The change is acquired by adding an optical film, i.e., a phase-shift adjustment layer (PSAL), onto the semitransparent electrode.

2. Model

Considering semitransparent electrodes of a device capped by an optical film, the multi-structure electrodes are substituted by an equivalent film to simplify the simulation, as depicted in Fig. 1. The phase change on the reflection from such an equivalent film is defined according to the complex reflection coefficient

$$r = \frac{\eta_0 - Y}{\eta_0 + Y} = |r| e^{i\varphi}. \quad (2)$$

Here, η_0 is the effective optical admittance of an organic layer adjacent to the equivalent thin film and η_0 is equal to $n_i(\lambda) \cos \theta_i$ and $n_i(\lambda) / \cos \theta_i$ for the *s*-polarization and *p*-polarization, respectively. $n_i(\lambda)$ is the refractive index of the organic layer adjacent to the top metal mirror

and θ_i is the angle inside the organic layer. Y is the complex optical admittance of this multilayer structure, which can be acquired by transfer matrix [9]. Thus, the phase changes of

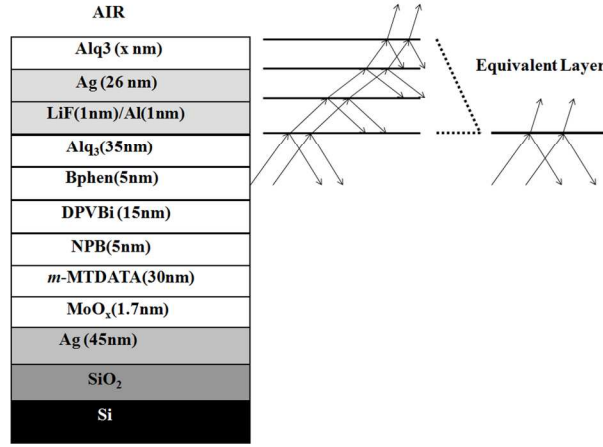


Fig. 1. Schematic diagrams of top-emitting devices and equivalent layers of multi-structure cathodes.

s -polarized and p -polarized light on the reflection from such a mirror are expressed by the following functions related to the thickness and refractive index of each capping layer [10]:

$$\varphi(d_r, n_r) \left\{ \begin{array}{l} \varphi^s = \tan^{-1} \left\{ \frac{2n_i(\lambda) \cos \theta_i [n_m(\lambda)y - k_m(\lambda)x]}{[n_m(\lambda)x + k_m(\lambda)y]^2 - n_i^2(\lambda) \cos^2 \theta_i^2 + [n_m(\lambda)y - k_m(\lambda)x]^2} \right\} \\ \varphi^p = \tan^{-1} \left\{ \frac{2n_i(\lambda) \cos \theta_i [n_m(\lambda)y + k_m(\lambda)x]}{n_i^2(\lambda)(x^2 + y^2) - [n_m^2(\lambda) + k_m^2(\lambda)] \cos^2 \theta_i^2} \right\} \end{array} \right\}, \quad (3)$$

of which s and p signify s -polarization and p -polarization, respectively. θ_{k+1} is the angle in the $k+1$ th layer, which is related to θ_i according to Snell's law, and $\cos \theta_i = x + yi$. For perpendicular incidence, the phase change of the s -polarization is in agreement with that of the p -polarization. And then, according to the model based on dipole radiation in a multilayer thin-film structure, the emission intensity in this direction can be given by [4, 11]

$$I(\lambda) = \frac{T_{\text{top}} \left[1 + R_{\text{bot}} + 2\sqrt{R_{\text{bot}}} \cos\left(\frac{4\pi z}{\lambda} - \varphi_{\text{bot}}\right) \right]}{1 + R_{\text{bot}} R_{\text{top}} - 2\sqrt{R_{\text{bot}} R_{\text{top}}} \cos\left(\frac{4\pi L}{\lambda} - \varphi_{\text{bot}} - \varphi_{\text{top}}(n_r, d_r)\right)} I_0(\lambda). \quad (7)$$

Here R_{bot} and R_{top} are the reflectance of the bottom metallic mirror and the top semitransparent mirror, respectively. z is the optical distance of the emitting dipoles to the bottom metallic mirror. Since the thickness of such an optical film is correlated to the phase shift on the reflection and emission intensity, it can be utilized properly to obtain a shorter emissive wavelength, even a blue emission.

In this paper, Alq₃ was used as the phase-shift adjustment layer, which is deposited onto a semitransparent electrode. To extract the effect of the thickness change of Alq₃ on the change

of the resonant wavelength straightforwardly, a simulation of the reflective phase change in the perpendicular direction with regard to the thickness of the capping layer is carried out first. Then an experiment based on simulation is executed.

4. Experiments

The device configuration used in our experiment as well as the schematic diagram of the equivalent layer was shown in Fig. 1. The optical constant of each layer referred to in the simulation was measured by ellipsometry. Before deposition of the metal electrode, the SiO₂ coated Si substrate was rinsed in a processing routine. Subsequently, a patterned 45 nm thick Ag was deposited on the substrate as an anode and bottom mirror, and then the sample was loaded into another evaporation chamber for organic deposition. 1.7 nm thick MoO_x was deposited first onto the Ag electrode as a buffer layer for better hole-injection capacity. Then, 30 nm thick 4,4',4''-tris(3-methylphenylphenylamino) triphenylamine (*m*-MTDATA), 5 nm thick N,N'-di(naphthalene-1-yl)-N,N'-diphenyl-benzidine (NPB), 15 nm thick 4,4'-bis(2,2'-diphenylvinyl)-1,1'-biphenyl (DPVBi), 5 nm thick 4,7-diphenyl-1,10-phenanthroline (Bphen), and 35 nm thick tris-8-hydroxyquinoline aluminum (Alq₃) were deposited in succession as the hole injecting layer, hole transporting layer, emitting layer, hole blocking layer, and electron transporting layer, respectively. All organic layers were deposited in a high vacuum of about 10⁻⁶ Torr and monitored by using an oscillating quartz thickness monitor *in situ*. 1 nm thick LiF was deposited as buffer layer without breaking the vacuum. Following the deposition of a 1 nm thick Al layer onto LiF, a 26 nm thick Ag cathode was deposited last to ensure the conductivity. For comparison, a counterpart bottom-emitting (BE) device was fabricated employing transparent Indium-Tin-Oxide (ITO) as the anode and the same cathode structure. The thickness of each layer used in the devices was emended by ellipsometry. Electroluminescent (EL) spectra, luminance yield, Commission International de l'Eclairage coordination (CIE_{x,y}), and *I-V* curves of the devices were measured by the system consisting of PR650 and Keithley 2400 in the atmosphere. The transmittance and reflectance of the multi-structure electrode were measured by an ultraviolet spectrophotometer.

5. Results and discussions

In Fig. 2, the phase shift on the reflection from a semitransparent cathode of LiF/Al/Ag is simulated as the thickness of the PSAL changes from 0 nm to 100 nm. It is obvious that the phase change on the reflection increases as the thickness of the PSAL of Alq₃ increases until it

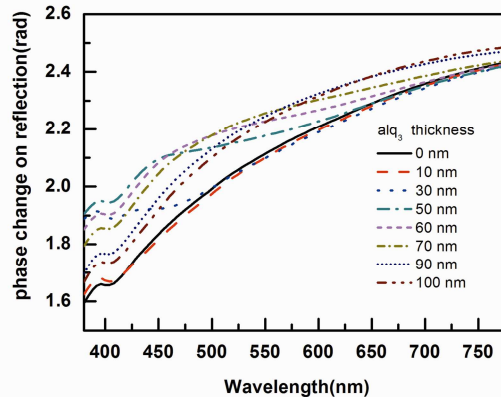


Fig. 2. Simulation of phase changes on the reflections of the top cathodes with various thicknesses of PSALs.

is 50 nm within the wavelength range of less than 500 nm. When the thickness increases further, the phase change begins to descend within the range of less than 460 nm, while it keeps on increasing within a wavelength range greater than 460 nm. The regular phase shift

indicates that the blue shift of a resonant wavelength caused by changing the thickness of the PSAL will take place in a certain range. By simulating the peak of emission spectra related to various thicknesses of PSALs and cavity lengths, which mean the physical thickness between two reflective electrodes, the change of the resonant wavelength is clearly presented. The peaks' changes in the simulation spectra of devices with PSALs of various thicknesses and cavity lengths are listed in Table 1. It is easily found that the peak of the resonant wavelength begins to shift to blue as the thickness of the PSAL increases until the thickness is 60 nm. If the thickness keeps on increasing, the resonant wavelength begins to move back. This phenomenon is consistent with the change of the phase shift on the reflection, and it also supports our deduction that the change of peak is definite for certain materials.

Table 1. Simulative Resonant Wavelengths and Maximum Shifts Associated with Different Thicknesses of PSALs and Cavity Lengths^a

Cavity length ^b	Thicknesses of PSALs								Maximum shift
	0	10	30	50	60	70	90	100	Δ_{\max}
80	468	468	464	456	456	456	460	464	12
90	496	496	488	480	476	484	488	492	20
100	528	528	520	508	508	512	520	520	20

^aUnit nm.

^bHere cavity length is the total thickness of organic layers sandwiched by two electrodes.

By analyzing the simulative data, it is also found that the maximum of change is different when different cavity lengths are adopted. According to Eq. (1), the expression for wavelength shift $\Delta\lambda$ on the perpendicular incidence can be obtained as follows:

$$\Delta\lambda = \frac{1}{\Delta\Phi} \left\{ \sum_i 4\pi d_i [n_i(0, \lambda + \Delta\lambda) - n_i(0, \lambda)] - \lambda(\Delta\varphi_{\text{top}} + \Delta\varphi_{\text{bot}}) \right\}, \quad (8)$$

$$\Delta\Phi = 2m\pi + \varphi_{\text{bot}}(0, \lambda + \Delta\lambda) + \varphi_{\text{top}}(0, \lambda + \Delta\lambda). \quad (9)$$

From these equations, it is found that the maximum wavelength shift is not only associated with the cavity length but also the phase change. However, a phase change on the reflection from the top electrode occurs in a certain range as the thickness of the PSAL changes. Then, a certain phase change will lead to a lesser wavelength change when a small cavity length is chosen. As a result, the maximum shift of the wavelength will also be reduced.

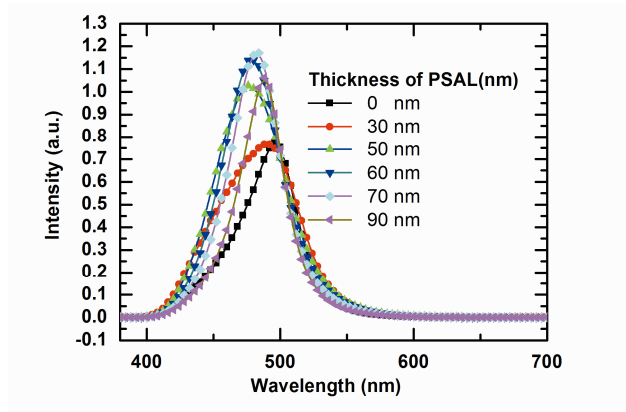


Fig. 3. Simulative emission spectra of top-emitting devices with cavity lengths of 90 nm.

Since Alq₃ is used as the PSAL in our simulation, the total thickness of the organic layer that determines the initial resonant wavelength must be in a certain range; otherwise, the shift of the resonant wavelength is not strong enough to obtain a blue emission. Accordingly, a device with a cavity length of 90 nm is adopted, and the simulative emission spectra are shown in Fig. 3. From Fig. 3 it is found that both the blue shift of the wavelength and the enhancement of spectra intensity are obtained. Based on the simulative emission spectra, the brightness is calculated according to the principle of radiometry and photometry. The calculated results are shown in Table 2. Though intensity of the emission spectra of the device with a 70 nm thick PSAL is the strongest according to Fig. 3, the brightness of the device with a 60 nm thick PSAL still is the highest after calculation using the vision function. Because the PSAL capped on the surface of the top-electrode is independent of the electricity characteristic, we suppose the device using a 60 nm thick PSAL will show the best performance.

Table 2. Simulative Brightness of a Top-emitting Device with Cavity Length of 90 nm

Thickness of PSAL (nm)	0	30	50	60	70	90
Brightness (cd/m ²)	8847	10630	10750	11060	9960	8594

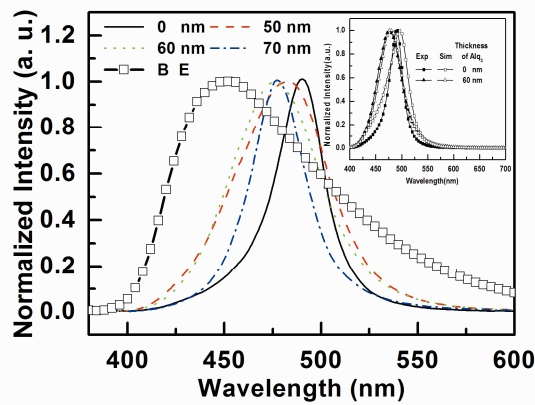


Fig. 4. Experimental emission spectra of a bottom-emitting device (open square) and a blue top-emitting device capped by various PSALs (solid line, 0 nm; dashed line, 50 nm; dotted line, 60 nm; dashed-dotted line, 70 nm). Inset: Comparison of numerical simulation spectra (open) and experimental (closed) emission spectra of devices without (square) and with (triangle) 60 nm thick Alq₃.

To confirm our numerical simulation, controlled devices with PSALs of various thicknesses were fabricated, and another counterpart bottom-emitting device was used for comparison. Figure 4 shows the electroluminescence (EL) spectra of these devices. It is now clear that the emission spectra shifts to blue since the PSAL is deposited onto the semitransparent cathode of the top-emitting device where the light is coupled out. The peak of the spectra changes to 484 nm from the original peak of 492 nm as the thickness of the PSAL reaches 50 nm. The spectra get a maximum shift of 16 nm as the thickness of the PSAL increases to 60 nm. The measured emission spectra are nearly in accordance with the simulation spectra, as shown in the inset of Fig. 4. The comparison of the photoluminescent (PL) spectra of Alq₃ and the emission spectra of devices with and without a 60 nm thick PSAL are made in Fig. 5 to ensure there is an excited emission of Alq₃. It is obvious that there is an overlap between the PL spectra of Alq₃ and the emission spectra of the device without a PSAL. This indicates that the energy transfer occurs when the light passes through Alq₃ when used as a PSAL. However, the weak absorbance of Alq₃ with such thickness as mentioned in our experiment leads to a very low conversion efficiency, and the excited emission of Alq₃ is

hardly observed in the emission spectra of a device with a 60 nm thick PSAL, as shown in Fig. 5.

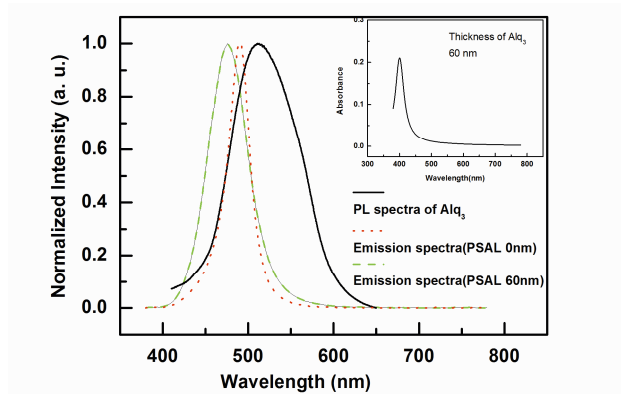


Fig. 5. Comparison of the PL spectra of Alq₃ and the emission spectra of an experimental device without and with a 60 nm thick Alq₃ PSAL. Inset: Absorbance curve of 60 nm thick Alq₃.

Accompanying the change in wavelength, the CIE_{x,y} of the device also shifts from (0.10 0.23) to (0.13 0.15) when the bias voltage is 8 V. It is better than the CIE_{x,y} of the counterpart bottom-emitting device (0.16, 0.16). If we keep on increasing the thickness of the PSAL to 70 nm, the peak of the spectra stays the same, while the full width at half-maximum is narrowed due to enhanced reflectance. Though it is beneficial for chromaticity of emissive light, the enhancement of reflectivity also impacts the luminescence of the device to a certain extent. As a result, the performance of a device using a PSAL with such thickness may be not as good as expected.

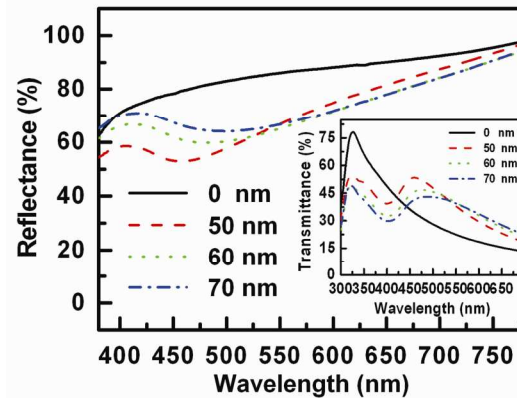


Fig. 6. Comparison of the experimental reflectance and transmittance (inset) of multi-structure cathodes (Al/Ag) capped by PSALs of various thicknesses.

The reflectance and transmittance changes associated with the thickness change, which is measured by an ultraviolet spectrophotometer, are shown in Fig. 6. It is apparent that when the thickness of the PSAL increases from 50 nm to 70 nm, the reflectance of the multi-structure electrode ascends gradually in the range of 380 to 500 nm. Nevertheless, the reflectances of those multi-structure electrodes are still better than that of a naked Ag electrode in the visible area. On the other hand, the transmittance descends simultaneously as the reflectance increases. But they are only better than that of a naked Ag electrode in the range of 450 to 780 nm. According to the measured curve, it is evident that the reflectance and transmittance of the multi-structure electrode is not improved strongly by a 60 nm thick PSAL

but is improved by a 50 nm thick PSAL. If the capping layer is used as an index-matching layer, 50 nm thick AlQ₃ may be the best choice. However, our final aim is to change the phase shift on the reflection to obtain the best blue emission. It is very different from the purpose of utilization of the capping layers, which has been reported by other researchers [12,13].

Figure 7 shows the current efficiency- and luminance-voltage characteristics of these controlled devices, respectively. The nearly identical current density of top-emitting devices with various thicknesses of PSALs indicates that the introduction of a PSAL is independent of the electrical characteristic of the device (see inset of Fig. 7), and it only affects the optical characteristics of the device. As a result, the device with a 60 nm thick PSAL shows excellent performance. The luminance and efficiency of the device reaches 20 000 cd/m² and 3.4 cd/A, respectively. Compared with a device using a 50 nm thick PSAL, the better performance is attributed to stronger magnification, which is related to the reflectance and transmittance of a semitransparent electrode in a microcavity. Additionally, the chromaticity is much better than that of a device using a 50 nm thick PSAL. Because of the lowest transmittance, the performance of a device using a 70 nm thick PSAL also is not as good as the device using a 60 nm thick PSAL, though it has better chromaticity. In comparison with a conventional bottom-emitting device, both the efficiency and the brightness of a top-emitting device using a 60 nm thick PSAL is higher. The top-emitting device using a PSAL, moreover, gives consideration to both efficiency and chromaticity, which is more acceptable for application.

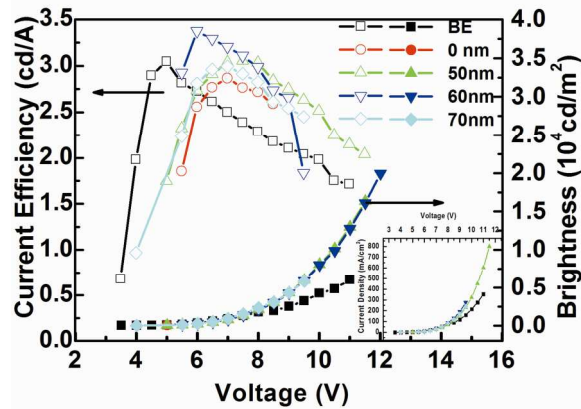


Fig. 7. Experimental current efficiency (left) and brightness (right) characteristics of the bottom-emitting device (BE) and top-emitting device with PSALs of various thicknesses. Inset: Corresponding voltage and current characteristics of devices.

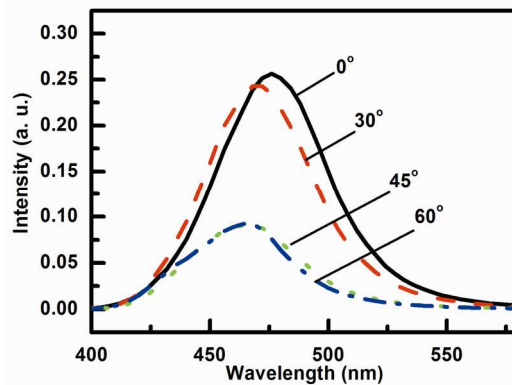


Fig. 8. Spectral dependence on viewing angles of device with 60 nm thick PSAL.

Figure 8 shows the dependence on viewing angles of the emission spectra of a controlled top-emitting device using a 60 nm thick PSAL. The dependence of the emission spectra is an important issue associated with such microcavity top-emitting devices. As the viewing angle changes from 0° to 60° , only a 12 nm blue shift of resonant wavelength finally occurs. Simultaneously, the $CIE_{x,y}$ changes from (0.13 0.15) to (0.14 0.09). The reason for less dependence on the viewing angle lies not only on the metallic reflective mirror but also on the bigger resonant wavelength than the intrinsic wavelength of the DPVBi [10,14].

6. Conclusion

In summary, the phase shift on the reflection from a semitransparent electrode can be adjusted by changing the thickness of the Alq_3 that is deposited onto the electrode. By simulation, it is found that the blue shift of the resonant wavelength caused by a change in the phase shift is definite with a certain cavity length. A blue top-emitting device has been acquired in our experiment via the proper design of the cavity length and the thickness of Alq_3 . Finally, the device using 60 nm thick Alq_3 as a phase adjustment layer shows a high current efficiency of 3.4 cd/A and a better $CIE_{x,y}$ of (0.13, 0.15). The brightness of the device reaches 20 000 cd/m^2 . The experiment results also confirm our conclusion obtained in the simulation. Such a method gives consideration to both efficiency and chromaticity. The results of this work will hopefully lead to brighter blue top-emitting devices for display applications based on microcavities.

Acknowledgments

The authors acknowledge financial support from the National Nature Science Fund Project under grants 60606017, 60706018, 60876032, and 60707016. We also thank the National High Technology Research and Development Program of China for financial support under grant 2006AA03A162, the National Nature Fund under grant 60723002, and the Research Fund for the Doctoral Program of Higher Education under grant 20070183088.